Journal of Molecular Structure 1213 (2020) 128152

Contents lists available at ScienceDirect

Journal of Molecular Structure

journal homepage: http://www.elsevier.com/locate/molstruc

Synthesis, characterization, biological, X-ray diffraction analysis and computational chemistry studies of new 2-acetylpyridine derivative hydrazone and its Zn(II) complex

Murat Çınarlı [a], Çiğdem Yüksektepe Ataol [b, *], Esra Çınarlı [c], Önder İdil [d]

[a] Central Research and Application Laboratory, Ahi Evran University, 40100, Kirsehir, Turkey
[b] Department of Physics, Faculty of Science, Cankiri Karatekin University, 18100, Cankiri, Turkey
[c] Department of Biology, Faculty of Science, Ahi Evran University, 40100, Kirsehir, Turkey
[d] Department of Basic Education, Faculty of Education, Amasya University, 05000, Amasya, Turkey

ARTICLE INFO

Article history:
Received 22 January 2020
Received in revised form
25 March 2020
Accepted 28 March 2020
Available online 7 April 2020

Keywords:
2-acetylpyridine
Single crystal
Hydrazone
Metal complex
Computational chemistry
DNA bases

ABSTRACT

A new aroyl hydrazone ligand ((E)-2-phenyl-N'-(1-(pyridine-2-yl)ethylidene)acetohydrazide) **HL** and its metal complex [ZnL_2] **(1)** have been synthesized and characterized by using elemental analysis, IR and UV−vis spectroscopy methods**.** All data indicate that the ligand is coordinated through enolate oxygen, pyridine nitrogen and the imine nitrogen in enolic form towards the metal ions. The single crystal X-ray diffraction analysis and Density Functional Theory (DFT) calculations were carried out for **HL** and **1** structures. **HL** and **1** crystallize in the monoclinic and the orthorhombic with P 2_1/n and P b c n space group with a = 5.2051(4) Å, b = 10.0477(9) Å, c = 25.204(2) Å, with a = 14.1300(18) Å, b = 9.3287(13) Å, c = 21.491(3) Å, respectively. The geometries, molecular orbital energies, and stability of the molecular structures were investigated in different solvent environments by using DFT/B3LYP/6-311G (d, p) method. Theoretical UV−vis spectra of the molecular structures were obtained and the percentage contributions of atomic orbitals of functional groups of the molecular structures to the molecular orbital energy levels were calculated in water media. The global reactivity parameters of the molecular structures were calculated and the interactions between the molecules with DNA bases such as adenine, cytosine, guanine, and thymine were investigated by using the ECT (Electrophilicity-Based Charge Transfer) method and ΔN (charge transfer) parameters. All the compounds were screened for antibacterial activity against Gram-positive, Gram-negative and yeast by using minimal inhibitory concentration method (MIC). [ZnL_2] **(1)** has been found to have more effect than **HL** in all microorganisms. Moreover, antioxidant activity was determined with the ABTS method. The DNA binding interactions was also determined experimentally by spectrophotometric and electrochemical methods.

1. Introduction

Aroylhydrazones have attracted the attention of many researchers in recent years due to their versatile uses (such as biological activity, strong chelating) [1–3]. Aroylhydrazones (>C═N−NH−CO−) are recognized by the presence of two inter-linked nitrogen atoms and they have an additional donor site like >C═O. The additional donor sites make them more flexible and versatile [4,5]. Such molecules show various biological effects [6–33]. Besides, 2-acetylpyridine is an important group in the structure of many drugs, and it is widely used as a starting material for many different chemical system studies [34]. Metal complexes of hydrazone derived from 2-acetylpyridine have received considerable attention over the past two decades [35]. This may be attributed to unusual structural features in the resultant metal complexes and their biological activities. Some of the metal complexes have antioxidative activities [35] and electronic and photophysical properties [36,37].

Because of these observations, we report the synthesis, characterization and biological activities of new 2-acetylpyridine derivative aroylhydrazone and its Zn(II) complex. The molecular structures of ligand **(HL)** and [ZnL_2] **(1)** complex have been

* Corresponding author.
E-mail addresses: yuksektepe.c@karatekin.edu.tr, yuksekc85@gmail.com (Ç. Yüksektepe Ataol).

https://doi.org/10.1016/j.molstruc.2020.128152
0022-2860/

determined by elemental analysis, IR and UV−vis. spectral studies and single crystal X-ray diffraction analysis. Besides, to compare experimental and theoretical results and to support experimental data, the molecular structures are optimized by using the DFT/B3LYP/6–311G(d, p) basis set in the gas, methanol, and water media. The molecular orbital energies, molecular electrostatic potential (MEP) map, and the global reactivity parameters of these compounds are calculated and also, the interactions between these compounds and DNA bases are determined by using the ECT (electrophilicity-based charge transfer) and ΔN (charge transfer) parameters. The antibacterial activity of the compounds to Gram-positive, Gram-negative, and yeast were measured.

2. Experimental

2.1. Materials

Phenylacetic hydrazide, $Zn(CH_3COO)_2 \cdot 2H_2O$ and Glacial acetic acid were obtained from Sigma-Aldrich. 2-Acetylpyridine and methanol were purchased from Merck Co. All chemicals purchased from commercial suppliers were reagent grade and were used without further purification.

2.2. Physical measurements and theoretical methods

The elemental analysis of the compounds was performed on a Thermo Flash 2000 Elemental Analyzer. The electronic absorption spectra of the title compounds were recorded at room temperature in the DMSO solution on a Thermo Evolution UV−Visible Spectrophotometer working between 200 and 1100 nm. IR spectra were recorded on a Thermo Scientific Nicolet iS10 FT- IR spectrophotometer using KBR disk. Starting geometries of the compounds were taken from X-ray refinement data for computing procedure. The molecular structures of the compounds in the ground state (in vacuo) were optimized by DFT methods to include correlation corrections with the polarized 6–311G(d, p) basis set in the gas, methanol and water media. DFT forms hybrid functionals, including B3 [38], which defines the exchange functional as the linear combination of Hartree-Fock, local, and gradient-corrected exchange terms. The B3 hybrid functional was used in combination with the correlation functionals [39]. The Highest Occupied Molecular Orbital (HOMO) and the Lowest Unoccupied Molecular Orbital (LUMO) of the molecules were obtained by single point energy calculation in the Ground State (GS) and gas, methanol and water media by using DFT/B3LYP/6–311G(d, p). And also, UV−vis spectra of the molecular structures were calculated by using (Time-Dependent) TD-DFT/B3LYP/6-311G(d, p) in the water media and the excited state. The global reactivity parameters were evaluated using equations given in the computational chemistry studies. The molecular structures and DNA bases were optimized and their energies were calculated by using DFT in water media.

All the calculations were performed using Gaussian 09 program [40].

2.3. X-ray crystallography

X-ray diffraction data of **HL** and **1** were collected at room temperature with Bruker APEX-II CCD diffractometer equipped with graphite-monochromated Mo-Kα radiation (λ = 0.71073 Å). The structures were solved by direct methods using SHELXT-2014/5 [41] implemented in the WinGX software system [42] and refined by the full-matrix least-squares procedure on F^2 using SHELXL-2018/3 for **HL** and SHELXL-2015/1 for **1** [43]. All non-hydrogen atoms were easily found from the difference Fourier map and refined anisotropically. All hydrogen atoms were included using a riding model and refined isotropically with CH = 0.93−0.97 Å and NH = 0.86 Å, $U_{iso}(H) = 1.2U_{eq}$ (1.5 for the methyl group) for **HL** and **1**, respectively. Crystallographic data of **HL** and **1**, details of the data collection and structure refinements are listed in Table 1.

2.4. Preparations

2.4.1. Synthesis of *(HL)*

Phenylacetic hydrazide (0.15 g, 1 mmol) was dissolved in methanol (20 mL). To this solution, 2-acetylpyridine (0.11 ml, 1 mmol) in methanol (20 mL) was added. The mixture was refluxed for 4−5 h and then left to cool. White color crystals were obtained in 2 days. Yield: 79%, Mp: 152 °C. Elemental Analysis, Found (Calc.) (%): C: 70.92 (71.13), H: 5.85 (5.97), N: 16.55 (16.59). The chemical structure of **HL** is shown in Scheme 1.

2.4.2. Synthesis of *(1)*

HL (0.0952 g, 0.4 mmol) was dissolved in methanol and a solution of $Zn(CH_3COO)_2.2H_2O$ (0.043 g, 0.2 mmol) in methanol was added to this solution. The reaction mixture was refluxed for 2−3 h and then left to cool. Pale yellow crystals suitable for X-ray analysis were obtained. Yield: 55%, Mp(decomp.): 274 °C. Elemental Analysis, Found (Calcd.) (%): C: 62.75 (63.22), H: 5.02 (4.95), N: 14.65 (14.74). The chemical structure of **1** is shown in Scheme 2.

2.4.3. Detection of antibacterial activity

The antimicrobial activities were tested against standard bacterial strains of Gram-positive (*Staphylococcus aureus* ATCC 6538P, *Bacillus cereus* ATCC 10876) and Gram-negative (*Escherichia coli* ATCC 25922, *Pseudomonas aeruginosa* ATCC 27853, *Salmonella typhimurium* LT2), yeasts (*Candida albicans* ATCC 10231) by using Minimal Inhibitory Concentration method (MIC). The compounds were dissolved in DMSO at the proper concentration. All cultures were incubated in nutrient broth at 37 °C for 24 h. Bacterial and yeast cells were suspended in 50 mL nutrient broth. The turbidity of bacterial and yeast suspensions was adjusted at a concentration of approximately 10^6 cells/ml by matching with 0.5 McFarland turbidity standards. Microorganisms were transferred 1 mL in test tubes and were added complexes. The incubation period of all the test cultures was 24 h at 37 °C in the incubator. The minimum inhibitory concentration, at which no growth was observed, was taken as the MIC value (μg/ml).

2.4.4. DNA interaction studies

pBR322 plasmid DNA cleavage activity of **HL** and **1** have been determined by agarose gel electrophoresis. The reactions were carried out in the presence and absence of 30 mM H_2O_2 as an activator. The concentration of ligand and complex were adjusted at 10 mM in DMSO and then treated with 0.25 ppm *pBR322* plasmid DNA. The final concentrations of the compounds were 1 mM. The DNA interaction reaction was carried out at room temperature for 24 h. After incubation period1 μl 6X gel loading buffer was added samples then loaded on 1% agarose gel for 90 min at 80 V in TBE buffer (pH 8). Gels were stained with ethidium bromide for 15 min and were washed deionized water for 15 min. Then gels were photographed under UV light.

2.4.5. Determination of antioxidant properties with ABTS method

The antioxidant properties of **HL** and **1** were evaluated by scavenging 2, 2′-azino-bis(ethylbenzthiazoline-6-sulfonic acid) radical cation ($ABTS^{\cdot+}$). For this purpose, $ABTS^{\cdot+}$ stock solution was prepared by mixing 7 mM ABTS solution with 2.45 mM potassium persulfate (KPS) solution 1: 1 (v:v) and incubating for 16 h. The $ABTS^{\cdot+}$ solution was diluted with distilled water to an absorbance

Table 1
Crystallograhic data for **HL** and **1**.

Molecules	**HL**	**1**
Empirical formula	$C_{15}H_{15}N_3O$	$C_{30}H_{28}N_6ZnO_2$
Molecular weight	253.30	569.95
Temperature, *T* (K)	296	296
Wavelength (Å)	0.71073	0.71073
Crystal system	Monoclinic	Orthorhombic
Crystal size (mm^3)	0.08 × 0.10 x 0.19	0.15 × 0.18 x 0.26
Space group	P 2_1/n	P b c n
a (Å)	5.2051(4)	14.1300(18)
b (Å)	10.0477(9)	9.3287(13)
c (Å)	25.204(2)	21.491(3)
α (°)	90.00	90
β (°)	91.675(4)	90
γ (°)	90.00	90
Volume, *V* ($Å^3$)	1317.6(2)	2832.9(6)
Z	4	4
Calculated density (Mg m^{-3}) μ (mm^{-1})	1.277 0.083	1.336 0.904
θ Range (°)	3.16–25.00	3.23–25.00
Index ranges	h = −6→6, k = −11 → 11, l = −29 → 29	h = −16 → 16, k = −11 → 11, l = −25 → 25
Measured reflections	25865	25612
Independent reflections	2305	2488
Observed reflections, (I > 2σ)	1696	1944
Goodness-of-fit on F^2	1.197	1.108
R_1 indices (I > 2σ)	0.09	0.05
wR_2 indices (I > 2σ)	0.17	0.11
CCDC Number	1842514	1861144

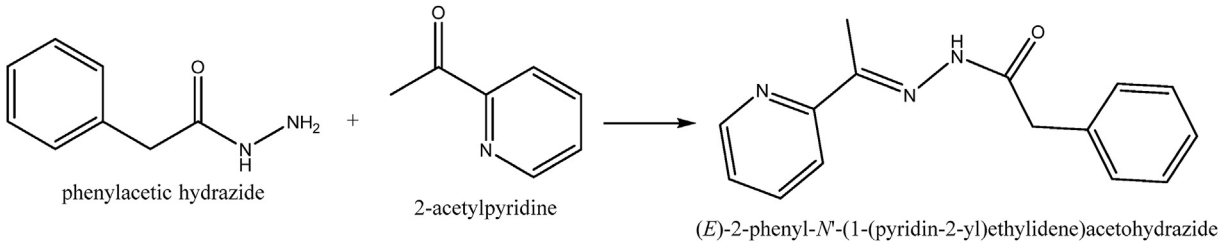

Scheme 1. Synthesis of **HL**.

of 0.700 (±0.02) at 734 nm. 20 μl of different concentrations of the compounds (0.78–50 mM) and 180 μl of $ABTS^{\cdot+}$ solution were mixed. After incubation for 15 min at room temperature and darkness, the absorbance at 734 nm was measured. Antioxidant capacity was determined using the following equation.

$$E = \left(\left(A_{sample} - A_{ABTS+} \right) / A_{ABTS+} \right) \times 100$$

A_{sample} and $A_{ABTS\cdot+}$ are the absorbance of the sample and $A_{ABTS\cdot+}$ solution, respectively. Butylated Hydroxy Anisole (BHA) was used as a standard antioxidant and the results were expressed as IC_{50} value. The IC_{50} corresponds to the concentration of the sample at the moment when half of $A_{ABTS\cdot+}$ is scavenging. The results were calculated from triplicate experiments.

3. Result and discussion

3.1. Structure description of *(HL)* and *(1)*

The molecular and single crystal structures of ((E)-2-phenyl-N'-(1-(pyridine-2-yl)ethylidene)acetohydrazide) **HL** and its metal complex [ZnL_2] **1** have been investigated by X-ray diffraction analysis. The molecular structures obtained from X-ray analysis results are shown in Figs. 1a and 2a, respectively. The selected bond parameters for the ligand and its metal complex structure are given in Table 2. The **HL** and **1** crystallize in monoclinic and orthorhombic space groups P 2_1/n and P b c n with a = 5.2051(4) Å, b = 10.0477(9) Å, c = 25.204(2) Å, with a = 14.1300(18) Å, b = 9.3287(13) Å, c = 21.491(3) Å, respectively. The Zn atom shows an almost octahedral N_4O_2 coordination sphere with the two ligands, meridionally oriented, coordinating the metal ion *via* the pyridine-N, hydrazone-N, and carbonyl-O atoms, the sum of the angle being 360.04°. **HL** in the keto form is transformed into an enolic form when it forms coordination. The compound **1** is coordinated pyridine nitrogen, carbonyl oxygen and imine nitrogen atoms of the tridentate enolic form of **HL**.

The ligand: the metal ratio was 2:1 for mononuclear **1** complex. As can be seen from Table 2, the C(8)–O(1) bond is a double bond in compound **HL** (1.227(4) Å), while it is converted to a single bond since the bond length is increased in bond **1** (1.250(5) Å). Likewise, the C(8)–N(2) bond is a single bond in **HL**, while it is converted to a double bond in **1**. The bond lengths C(8)–O(1) and C(8)–N(2) are agreeable with the literature [44–53]. According to the results of X-ray diffraction, it can be said that compound **HL** is transformed to enol form from keto form when complex is formed. The torsion angle C(6)–N(1)–N(2)–C(8) is approximately planar and its value is −177.7(3)° for **HL** and 174.3(3)° for **1**.

The compound **HL** has intermolecular N–H…O hydrogen bond while the classic hydrogen bonds can not be observed in compound

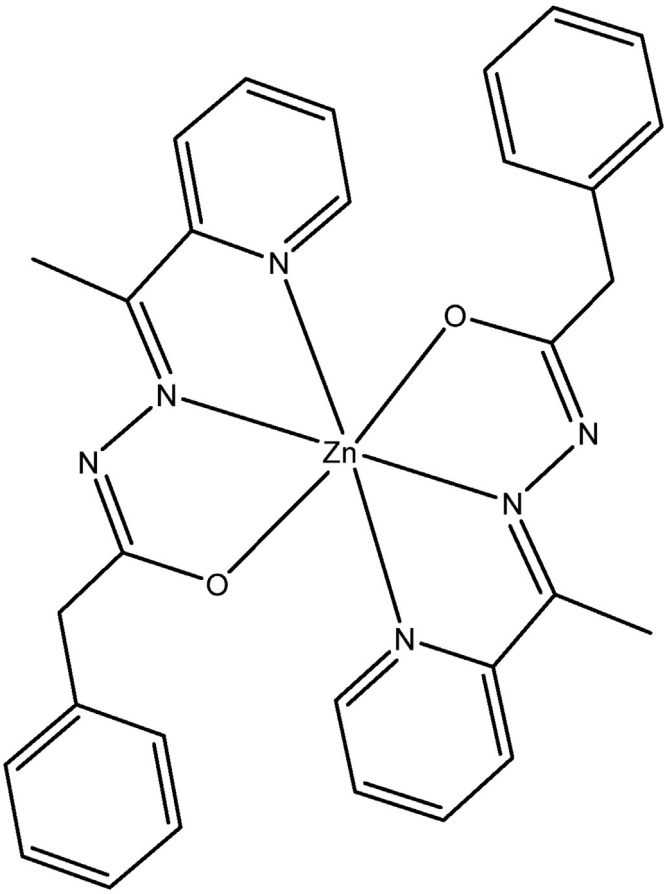

Scheme 2. Chemical structure of **1**.

1. The intermolecular hydrogen bond can be seen in Fig. 3 and Table 3. The atom hydrazone-N(2) of the molecule at (x, y, z) acts as hydrogen-bond donor, *via* atom H(2A), to atom carbonyl-O(1) of the molecule at (2-x, 2-y, -z), so generating by inversion a dimer, by an $R_2^2(8)$ motif (see Fig. 3). The $R_2^2(8)$ rings formed by hydrogen bonds are centered at both [n+1/2, k+1/2, l+1/2] and [n, m, k] (n, k, and l are zero or integer) in the monoclinic cell. These rings, like the body-centered structure, are centered both in the middle of the unit cell and at the corner points forming the crystal package structure (see Fig. 3).

3.2. IR studies of **(HL)** and **(1)**

In the IR spectra of **HL**, the bands at 3201 cm^{-1}, 1665 cm^{-1}, 1599 cm^{-1}, 1577 cm^{-1}, and 1045 cm^{-1} are due to ν(N-H), ν(C═O), $\nu(C{=}N)_{azo.}$, $\nu(C{=}N)_{pyr.}$, and ν(N-N), respectively. The IR spectrum of **1** shows significant changes compared to that of the ligand. In the complex, the bands of ν(N-H) and ν(C═O) disappear. The amide proton is deprotonated with complexation [54,55]. In the complex spectrum, two new bands due to conjugate system ν(>C= N-N═ C<) and $\nu(C\text{-}O^-)$ appeared at 1564 cm^{-1} and 1256 cm^{-1}, respectively. On complex formation, the bands of $\nu(C{=}N)_{azo.}$ and $\nu(C{=}N)_{pyr}$ are shifted to the higher wavenumbers, shift which indicates that the azomethine and pyridine nitrogen atoms are coordinated to the metal ion (Fig. 4).

3.3. UV–vis. Studies of **(HL)** and **(1)**

The **HL** ligand shows peaks at 290 nm ($\varepsilon = 20880$ $Lmol^{-1}cm^{-1}$) and 295 nm ($\varepsilon = 21020$ $Lmol^{-1}cm^{-1}$), which may be attributed to the $\pi \rightarrow \pi^*$ transitions of its position and molar absorption coefficient. In the UV–vis spectra of **HL**, intra-ligand $\pi \rightarrow \pi^*$ transitions were almost unchanged. In the Uv–vis spectra of **1**, the charge transfer transition was observed at 358 nm (2250 $Lmol^{-1}cm^{-1}$) (see Fig. 5) [56,57].

3.4. Antimicrobial activity of **(HL)** and **(1)**

Antimicrobial effect of **HL** and **1** was investigated in this study according to Minimal Inhibitory Concentration (MIC) method and it was found that DMSO used as Control had no significant effect on microorganisms (5000 μg/ml). However, it was determined that ligand and complex have significant effects on microorganisms. The MIC values for the **HL** were 93.79 μg/mL for gram-negative *Escherichia coli* and gram-positive *Bacillus cereus*, as well as 3000 and 1500 μg/ml for other gram-negative and gram-positive bacteria (see Table 4). When the MIC values of **1** are examined, it is seen that these values are 11.71 μg/ml for gram negative *Pseudomonas aeruginosa* and *Escherichia coli*, *Bacillus cereus* and *Staphylococcus aureus* for gram positive and 93.79 μg/ml for gram negative *Salmonella typhimurium*. Copper and zinc ions are known to have three main mechanisms for antimicrobial activity [58,59]. First, metal ions bind to proteins to neutralize microorganisms. Second, metal ions can interact with the vital membrane for microorganisms. Thirdly, metal ions interact with microbial nucleic acids and affect microorganisms. The antimicrobial effect seen here can be explained by the relationship of complexes with the cell wall. The cell wall

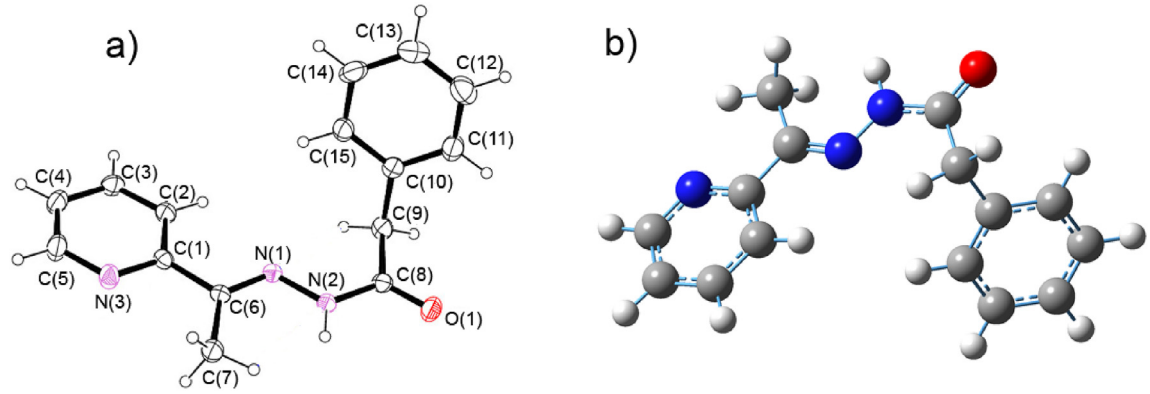

Fig. 1. The molecular structure of **HL**. a) for X-ray result. Anisotropic displacement ellipsoids are drawn at the 50% probability level, b) for the optimized molecular structure **HL** by using B3LYP/6-311G(d, p) in methanol media.

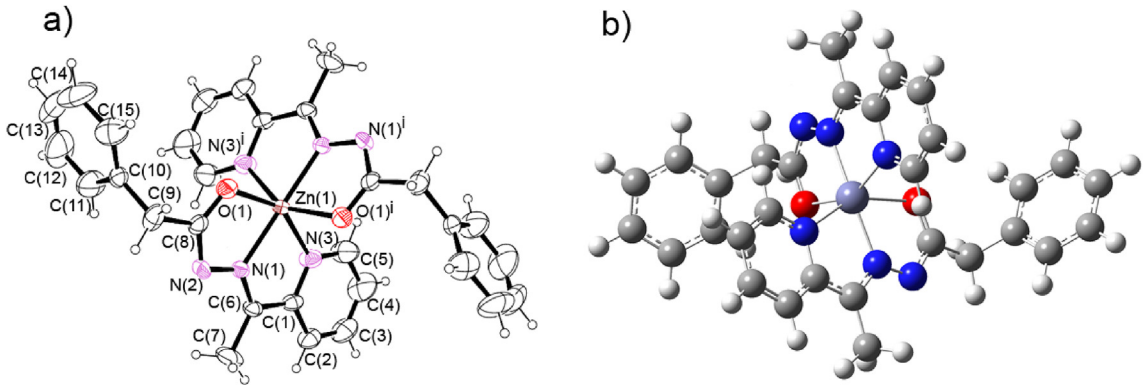

Fig. 2. The molecular structure of **1**. a) for X-ray result. Anisotropic displacement ellipsoids are drawn at the 50% probability level, b) for the optimized molecular structure **1** by using B3LYP/6-311G(d, p) in water media. (Symmetry code: (i) 1-x, y, ½-z).

Table 2
The selected some bond parameters of the compound **HL** and **1** (Symmetry code: (i) 1-x, y, ½-z).

	HL	1	HL			1		
	Exp.	Exp.	B3LYP 6−311G (d, p)	B3LYP 6−311G (d, p) Water	B3LYP 6−311G (d, p) Methanol	B3LYP 6−311G (d, p) Gas	B3LYP 6−311G (d, p) Water	B3LYP 6−311G (d, p) Methanol
Bond Lengths (Å)								
N(1)−N(2)	1.377(4)	1.368(4)	1.353	1.357	1.357	1.363	1.363	1.363
N(1)−C(6)	1.281(4)	1.280(4)	1.289	1.289	1.289	1.341	1.340	1.341
N(2)−C(8)	1.347(4)	1.334(5)	1.386	1.377	1.377	1.359	1.355	1.356
C(8)−O(1)	1.227(4)	1.252(5)	1.216	1.222	1.223	1.237	1.242	1.242
N(3)−C(1)	1.336(4)	1.346(5)	1.341	1.342	1.342	1.387	1.391	1.391
N(3)−C(5)	1.334(5)	1.329(6)	1.335	1.337	1.337	1.337	1.340	1.340
C(1)−C(6)	1.488(5)	1.473(6)	1.488	1.490	1.490	1.427	1.428	1.428
Zn(1)−N(1)	–	2.062(3)	–	–	–	2.040	2.035	2.035
Zn(1)−O(1)	–	2.124(3)	–	–	–	2.385	2.374	2.376
Zn(1)−N(3)	–	2.203(3)	–	–	–	2.100	2.110	2.109
R^2			0.9355	0.9599	0.9602	0.9391	0.9439	0.9430
Bond Angles (°)								
N(1)−N(2)−C(8)	121.0(3)	108.5(3)	123.86	123.44	123.30	117.79	117.57	117.58
N(2)−N(1)−C(6)	117.3(3)	120.5(3)	118.40	118.28	118.27	121.37	121.60	121.58
N(2)−C(8)−O(1)	120.2(3)	127.1(4)	119.03	119.27	119.27	120.84	120.57	120.59
O(1)−C(8)−C(9)	121.6(3)	118.0(4)	123.30	122.78	122.86	122.84	122.89	122.91
N(1)−C(6)−C(1)	116.1(3)	115.1(3)	116.53	116.16	116.19	114.63	114.34	114.36
C(6)−C(1)−N(3)	115.4(3)	115.1(3)	116.59	116.69	116.70	115.89	115.99	115.99
C(1)−N(3)−C(5)	118.1(3)	118.2(4)	118.54	118.49	118.49	119.26	119.10	119.11
C(8)−C(9)−C(10)	111.5(3)	113.2(3)	111.35	111.05	111.50	112.60	112.07	112.11
O(1)−Zn(1)−N(1)	–	74.79(11)	–	–	–	72.57	72.52	72.50
O(1)−Zn(1)−N(3)	–	149.51(12)	–	–	–	150.05	149.79	149.81
N(1)−Zn(1)−N(3)	–	74.78(12)	–	–	–	77.76	77.51	77.53
O(1)−Zn(1)−O(1)^i	–	97.54(17)	–	–	–	84.58	86.04	85.96
O(1)−Zn(1)−N(1)^i	–	103.78(11)	–	–	–	95.28	97.82	97.65
O(1)−Zn(1)−N(3)^i	–	91.47(13)	–	–	–	94.32	94.49	94.51
N(1)−Zn(1)−N(1)^i	–	177.90(17)	–	–	–	163.87	167.10	166.86
N(1)−Zn(1)−N(3)^i	–	106.69(12)	–	–	–	112.99	111.17	111.29
N(3)−Zn(1)−N(3)^i	–	95.37(19)	–	–	–	100.92	99.74	99.73
R^2			0.9063	0.9256	0.9267	0.9283	0.9475	0.9464

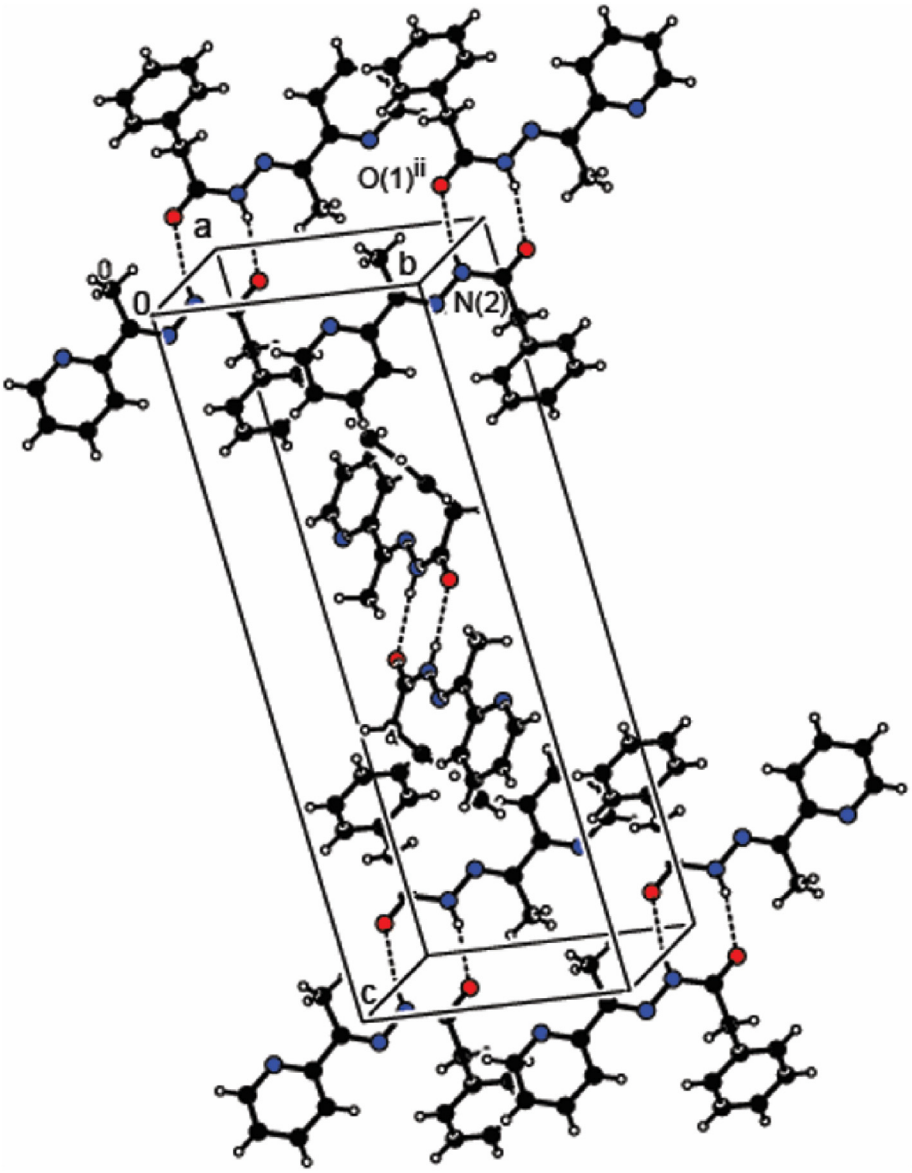

Fig. 3. A partial packing diagram of **HL**, hydrogen bonding interactions have been shown as broken lines. (Symmetry code: (ii) 2-x, 2-y, -z).

Table 3
Hydrogen bond parameters of **HL**.

D–H···A	D–H(Å)	H···A(Å)	D···A (Å)	D–H···A (°)
N(2)–H(2A)...O(1)^{ii}	0.86	2.24	3.087(4)	168

D = Donor, H= Hydrogen, A = Acceptor, Symmetry code: (ii): 2-x, 2-y, -z.

structure, especially the peptidoglycan layer, is vital for the survival of many bacteria. Therefore, some antibiotics act by inhibiting a step of peptidoglycan synthesis [60]. As a result, it is seen that the new complex synthesized has a very high antimicrobial effect.

3.5. DNA cleavage studies of *(HL)* and *(1)*

DNA Cleavage activity of compounds was evaluated by conversion of pBR322 DNA supercoiled form to nicked circular and linear form.50 mM Tris–HCl (pH: 8) (Fig. 6 Lane 1) and DMSO (Fig. 6 Lane 2) were used as control groups. The results of the agarose gel electrophoresis were shown in Fig. 6. **HL** (Fig. 6 Lane 3) and (Fig. 6 Lane 4) **1** didn't show any cleavage activity on *pBR322* plasmid DNA absence of H_2O_2. The percentage of form II increased in the presence of hydrogen peroxide (Fig. 6 Lane 5). In the presence of hydrogen peroxide and DMSO, plasmid DNA is normal due to its scavenging activity of DMSO (Fig. 6 Lane 6). **HL** didn't show any activity in the presence of hydrogen peroxide (Fig. 6 Lane 7). While the percentage of nicked circular DNA increased, whereas the percentage of linear form decreased in the presence of hydrogen peroxide and 1 mM complex **1** (Fig. 6 Lane 8).

3.6. Antioxidant activity studies of *(HL)* and *(1)*

The IC50 values of Butylated hydroxyanisole (BHA), **HL** and **1** were 0.209 (±0.006), 17.51 (±0.41) and 42.29 (±0.37) mM, respectively. Ligand and its [ZnL_2] complex showed lower antioxidant properties compared to Butylated hydroxyanisole (BHA). When the ligand formed a complex with zinc, it was found that the antioxidant capacity decreased.

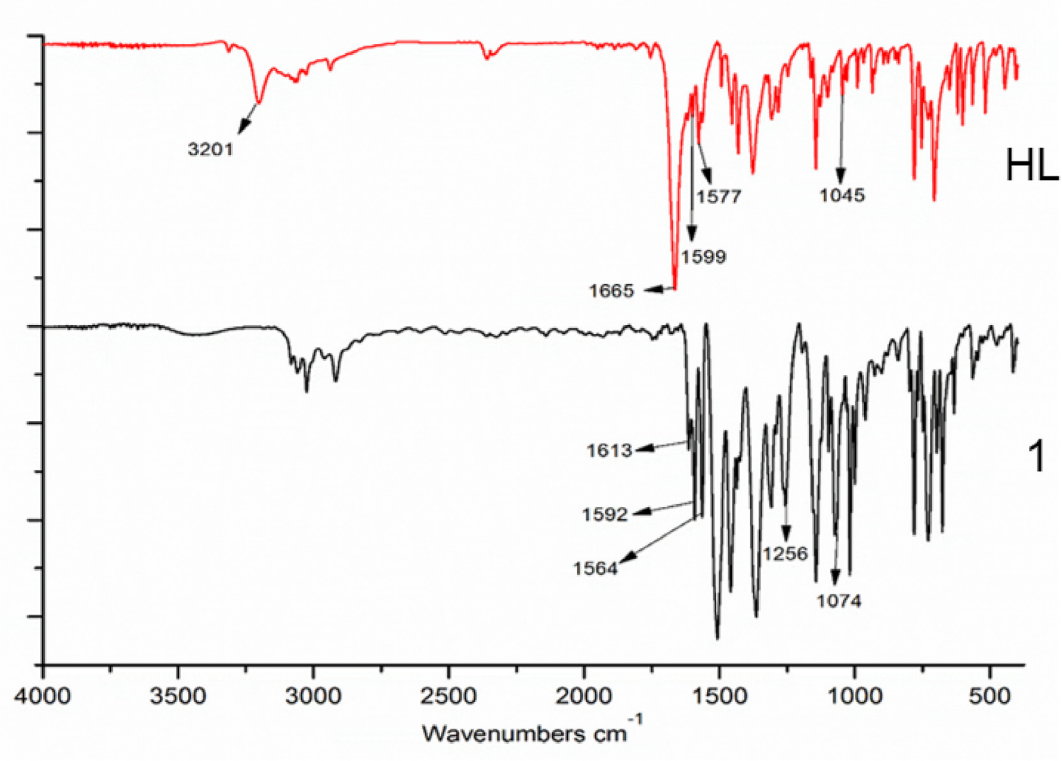

Fig. 4. IR spectra of the compounds.

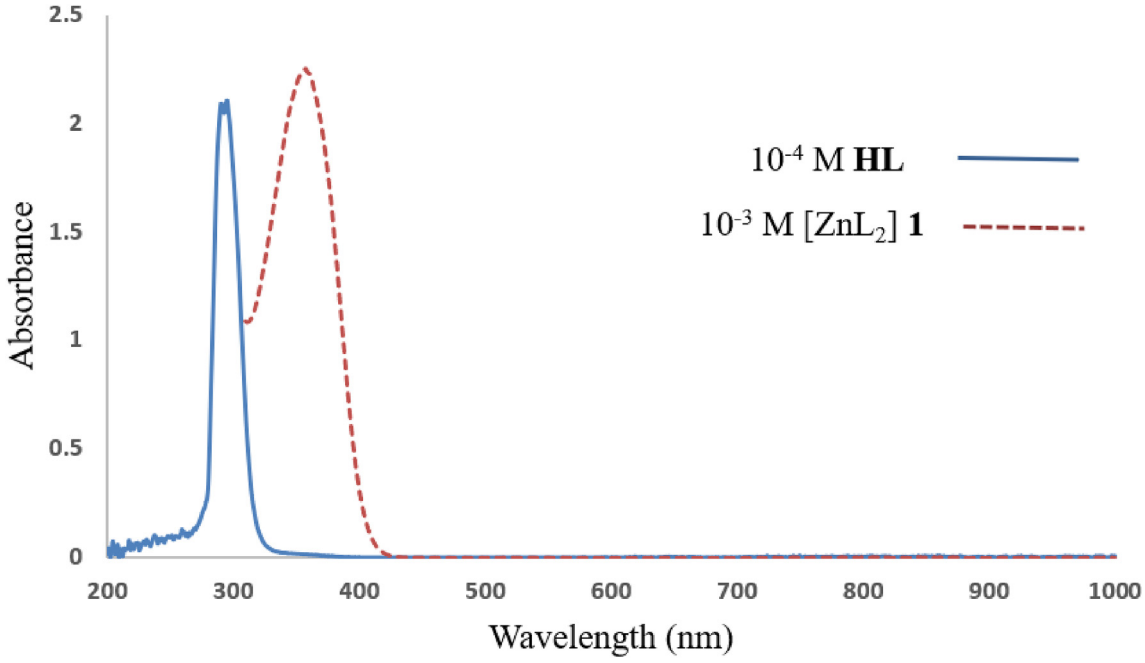

Fig. 5. Absorption spectra of **HL** and **1**.

3.7. *Computational chemistry studies of **(HL)** and **(1)***

In this study, firstly, molecular structures of the compounds **HL** and **1** have been optimized in the ground state both in the gas and in different solvent environments (methanol and water) with the DFT/B3LYP/6-311G(d, p) method and its appropriate geometries have been obtained. Some calculated the bond parameters are given in Table 2 and the comparison with experimental values was done by R^2 (a measure of goodness-of-fit of linear regression) regression analysis method. According to the results of the regression analysis, the compatibility graphs between the experimental and the calculated values for **HL** and **1** can be seen in Figs. 7 and 8.

According to Table 2, we can be said that the results obtained in

Table 4
MIC values of **HL** and **1**.

	Pseudomonas aeruginosa ATCC 27853	*Escherichia coli* ATCC 25922	*Salmonella typhimurium* LT2	*Bacillus cereus* ATCC 10876	*Staphylococcus aureus* ATCC 6538P	*Candida albicans* ATCC 10231
HL	3000	93.79	1500	93.79	3000	23.43
1	11.71	11.71	93.79	11.71	11.71	23.43
DMSO	>5000	>5000	>5000	>5000	>5000	>5000

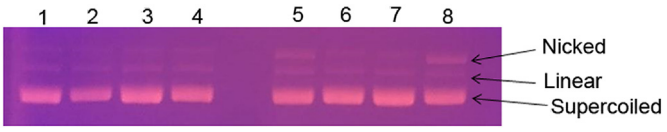

Fig. 6. Cleavage of pBR322 plasmid DNA by **HL** and **1** absence and presence of H_2O_2. Lane 1: pBR322 DNA control in 50 mM Tris-HCl buffer (pH: 7.2) Lane 2: pBR322 DNA+DMSO control Lane 3: pBR322 DNA + 1 mM **HL** Lane 4: pBR322 DNA+ 1 mM (**2**) Lane 5: pBR322 DNA + 30 mM H_2O_2control Lane 6: pBR322 DNA+DMSO + 30 mM H_2O_2 control Lane 7:pBR322 DNA + 1 mM (**1**) + 30 mM H_2O_2 Lane 8: pBR322 DNA+ 1 mM **1** + 30 mM H_2O_2.

the methanol and water media are more compatible with experimental bond parameters for **HL** and **1**, respectively. Figs. 9 and 10 show the superimpositions of the molecular structures obtained from the calculation results and the X-ray diffraction analysis results.

Secondly, the energies of molecular structures are calculated in both gas and solvent environments with a single point energy calculation, and total energies, molecular orbital energies, molecular electrostatic potential maps and the global reactivity parameters of **HL** and **1** are obtained by using DFT/B3LYP/6-311G(d, p). Besides, the interactions between the molecular structures with DNA bases were investigated by using the global reactivity parameters. In addition to these studies, UV−vis spectra of molecular structures were also obtained with TD-DFT and the transitions between the molecular levels were investigated.

The highest occupied molecular orbital by electrons is HOMO and the lowest non-occupied by electrons molecular orbital is LUMO. HOMO and LUMO energy values, total energies of **HL** and **1** are calculated in the ground state both gas and methanol with water media. The dielectric constants and dipole moments of the solvent media are given such as Methanol $\varepsilon = 32.7$, $\mu = 1.7$; Water $\varepsilon = 80.1$, $\mu = 1.82$. The greater the dielectric constant, the greater the polarity. The energy values of **HL** and **1** are given in Table 5. As can be seen from Table 5, the lowest total energy values for both molecular structures were obtained from the water environment. According to the result obtained, we can say that both structures are more stable in the water environment. Molecular orbital energy diagrams of molecular structures, percent distributions of atomic orbitals to molecular orbital energy levels of the molecular structure and the distribution of bond and anti-bond electrons to HOMO and LUMO levels are given in Figs. 11 and 12.

According to Figs. 11 and 12, for **HL** and **1**, we can say that the more contribution to the HOMO level comes from the hydrazone group while the more contribution to the LUMO level comes from the pyridine ring.

UV−vis spectra of the molecular structures are calculated by using TD-DFT/B3LYP/6-311G(d, p) in the water media and the excited state. The calculated some absorption wavelengths and the molecular orbital transitions are given in Table 6 and UV−vis spectra of **HL** and **1** is given in Fig. 13. Absorption peaks at 290 nm for **HL** and 358 nm for **1** in the experimental UV−vis spectra were observed in the DMSO environment. According to the results of the theoretical calculation, transitions from 91% from HOMO to LUMO at 289 nm for **HL** and 81% HOMO-1 to LUMO at 358 nm for **1** are observed.

The single point energy calculations of **HL** and **1** are performed

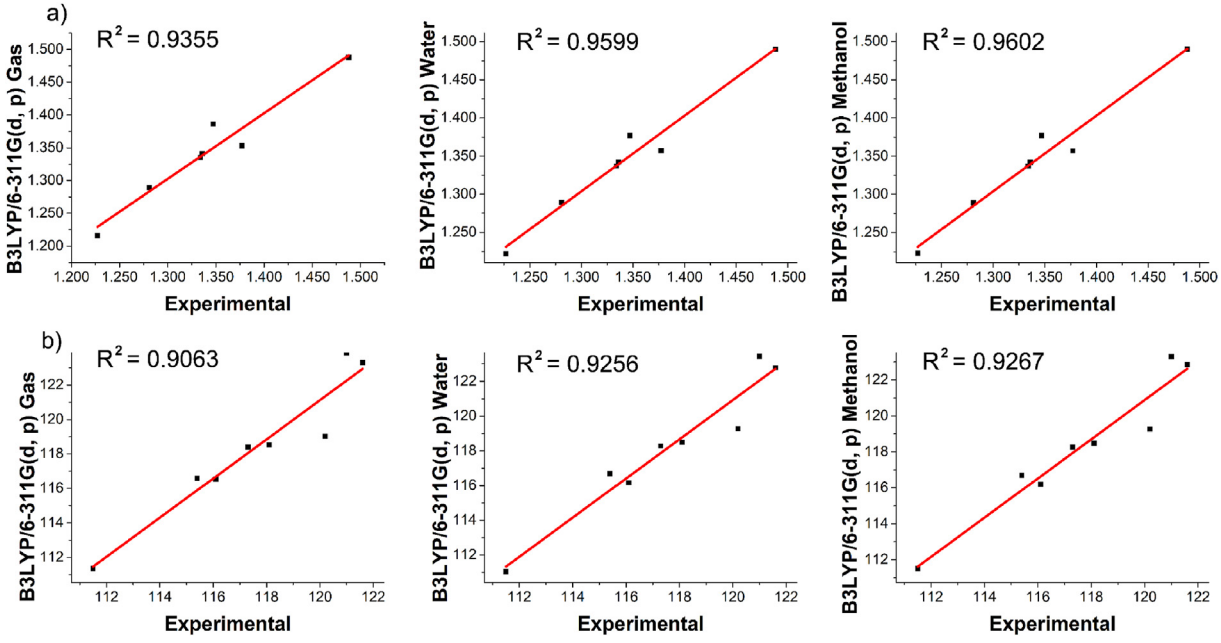

Fig. 7. The regression analysis results of the optimized molecular structure **HL**, **a)** for the bond lengths, **b)** for the bond angles.

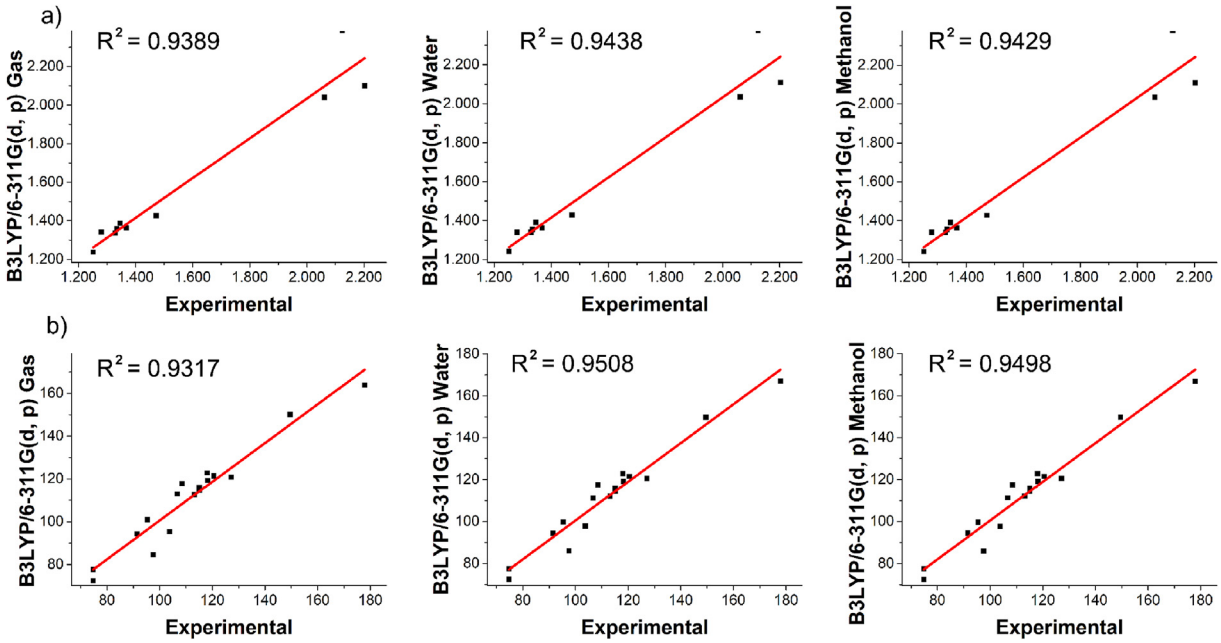

Fig. 8. The regression analysis results of the optimized molecular structure **1**, **a)** for the bond lengths, **b)** for the bond angles.

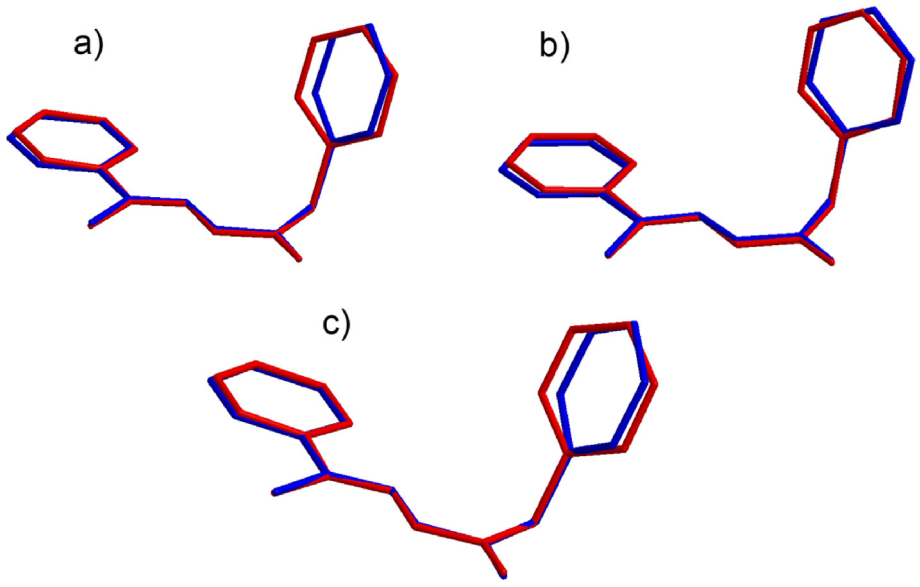

Fig. 9. Atom-by-atom superimposition of **HL** calculated (blue) by B3LYP/6–311G(d, p) over the X-ray structure (red) for**, a)** X-ray with the gas, **b)** X-ray with the water, **c)** X-ray with the methanol.

by using DFT/B3LYP/6-311G(d, p) and their Molecular Electrostatic Potential (MEP) maps are obtained. The MEP surface of a molecule identifies its chemically active regions [61]. It is very important to understand the nucleophilic, electrophilic regions of the molecule and to define intra and intermolecular interactions. Red regions on the potential energy surface define more nucleophilic regions, and blue regions define more electrophilic regions. MEP surface of **HL** and **1** is given in Fig. 14. As can be seen from Fig. 14, in both **HL** and **1**, we can say that the region where the carbonyl oxygen and pyridine nitrogen atoms are nucleophilic and the region where the hydrazone nitrogen and hydrogen methyl atoms are electrophilic. These atoms act as donor/acceptor in the intra/intermolecular interactions.

To investigate the interaction between DNA bases with **HL** and **1** the molecular structures **HL** and **1** with DNA bases (adenine, cytosine, guanine, and thymine) are optimized by using B3LYP/6−311G(d, p) method in the ground state and water media. And then, using the optimized structures, their HOMO and LUMO energies are obtained with the single point energy calculations by B3LYP/6−311G(d, p) method in water media. The global reactivity parameters of the adenine, guanine, cytosine, thymine and the molecular structures are derived from their HOMO and LUMO energy values.

The global reactivity parameters were evaluated using equations given. ECT (electrophilicity-based charge transfer) method and ΔN (charge transfer) parameters were used to determine the

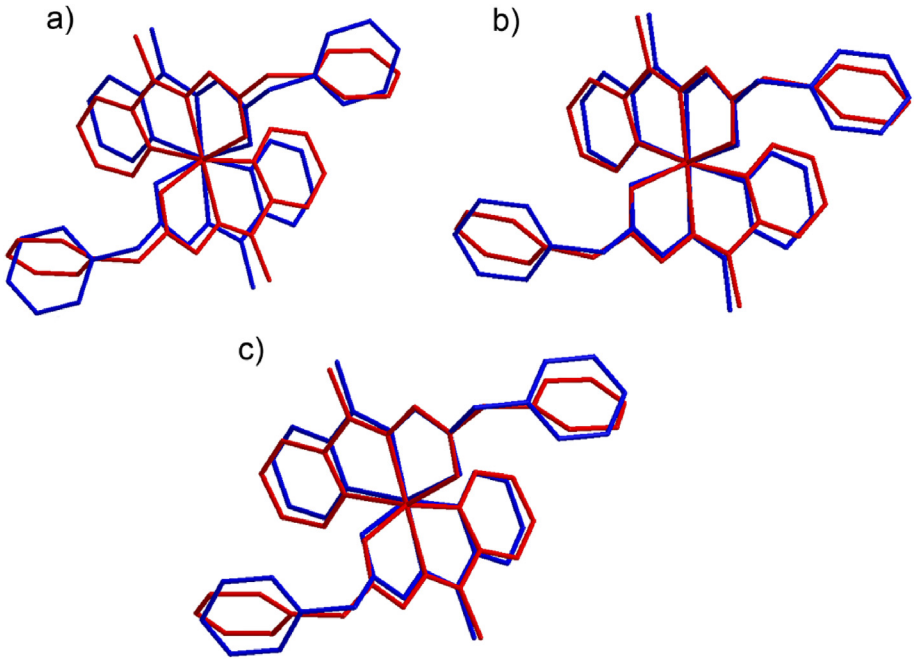

Fig. 10. Atom-by-atom superimposition of **1** calculated (blue) by B3LYP/6–311G(d, p) over the X-ray structure (red) for, **a)** X-ray with the gas, **b)** X-ray with the water, **c)** X-ray with the methanol.

Table 5
The calculated molecular orbital energies of the molecular structures. The dielectric constants and dipol moments of the solvent media are given such as Methanol $\varepsilon = 32.7$, $\mu = 1.7$; Water $\varepsilon = 80.1$, $\mu = 1.82$

B3LYP	E_{HOMO} (eV)	E_{LUMO} (eV)	μ (D)	Total Energy (a.u.)	ΔE (eV)
6-311G(d, p) Gas for **HL**	−6.4094	−1.8166	3.6504	−820.30495	4.5928
6-311G(d, p) Methanol for **HL**	−6.4532	−1.8215	4.9211	−820.31617	4.6317
6-311G(d, p) Water for **HL**	−6.4587	−1.8226	4.9803	−820.31660	4.6361
6-311G(d, p) Gas for **1**	−2.6020	−1.9489	2.7021	−3419.98227	0.6531
6-311G(d, p) Methanol for **1**	−2.9154	−2.2545	2.7332	−3419.98100	0.6609
6-311G(d, p) Water for **1**	−2.9331	−2.2730	2.7021	−3419.98227	0.6601

interactions between these structures and DNA bases. According to the Density Functional Theory [62,63], the vertical ionization potential (*IP*) and the electron affinity (*EA*) of the molecule are defined as

$$IP = -E_{HOMO} \tag{1}$$

$$EA = -E_{LUMO} \tag{2}$$

$$\chi = -\mu \tag{3}$$

where E_{LUMO} is the lowest unoccupied molecular orbital's energy and E_{HOMO} is the highest occupied molecular orbital's energy in Eqs. (1) and (2) and χ (eV) in Eq. (3) is the electronegativity. The electronegativity (χ) is equal to the negative value of the chemical potential (μ). The electronegativity (χ) and chemical hardness (η) of the molecule are defined as

$$\chi = (1/2)(IP + EA) \tag{4}$$

$$\eta = (1/2)(IP - EA) \tag{5}$$

The electrophilicity index (ω) and global softness (S) are defined as follows:

$$\omega = \frac{\mu^2}{2\eta} \tag{6}$$

$$S = \frac{1}{2\eta} \tag{7}$$

The global interactions between the molecular structures and DNA bases have been determined using the parameter ΔN, which represents the fractional number of electrons, transferred from system A to system B, and is represented by [64,65].

$$\Delta N = \frac{\mu_B - \mu_A}{2(\eta_A + \eta_B)} \tag{8}$$

where μ_A, μ_B, and η_A, η_B are the chemical potentials and chemical hardnesses of systems A and B, respectively. If $\Delta N < 0$, charge flows from A to B (A acts as an electron donor), and if $\Delta N > 0$, charge flows from B to A (A acts as an electron acceptor). Associated with the definition of global electrophilicity, there is an additional and useful relationship that accounts for the maximum electronic charge ΔN_{max} that the electrophile may accept from the environment. Here, the environment may be represented by either external effects coming, for instance, from the interaction with the solvent or more simply as field effects coming from the presence of substituent groups in the molecule.

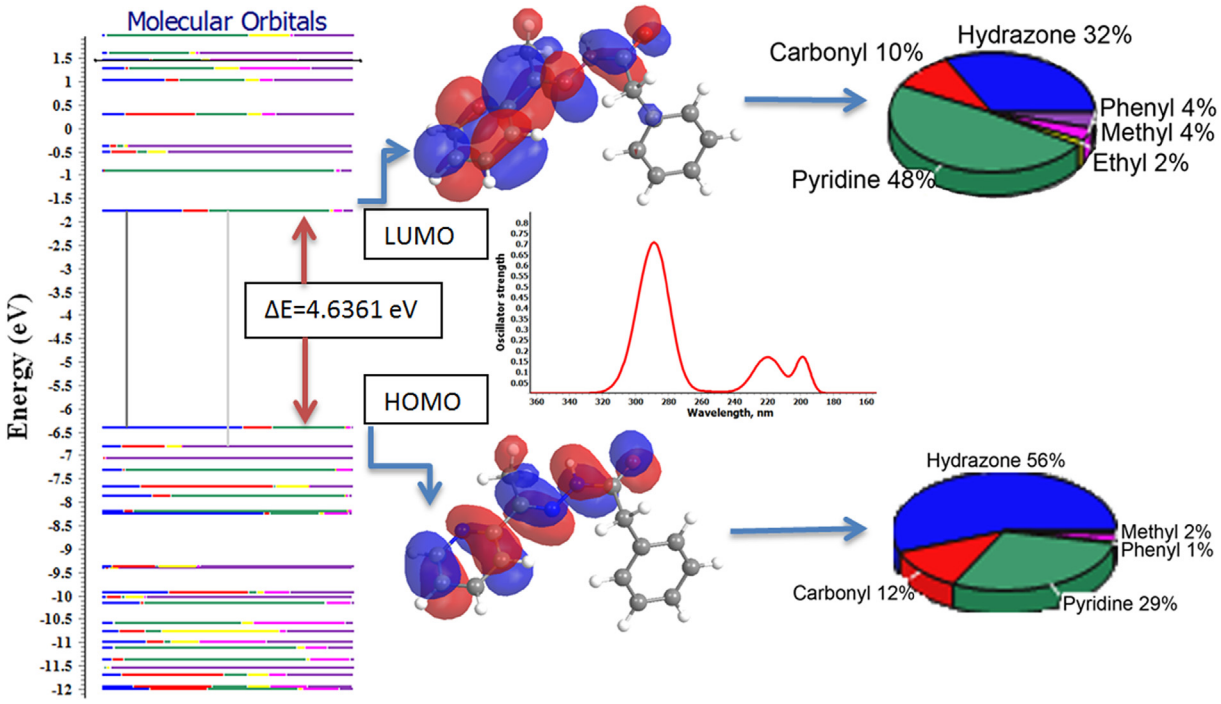

Fig. 11. The molecular orbital energies of **HL** in the water media by B3LYP/6-311G(d, p).

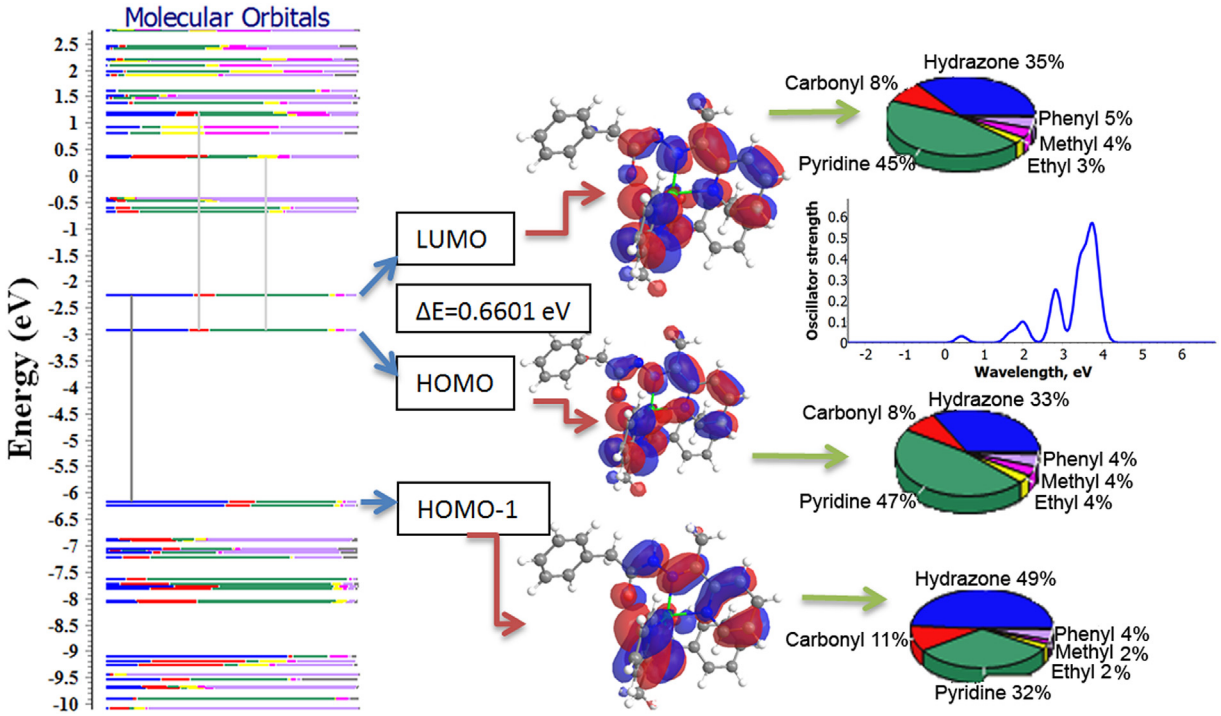

Fig. 12. The molecular orbital energies of **1** in the water media by B3LYP/6-311G(d, p).

ΔN_{max} has been defined as [65].

$$\Delta N_{max} = -\mu/\eta \tag{9}$$

Electrophilicity of a system can be written in terms of ΔN_{max} as follows:

$$\omega = \mu^2/2\eta = (-\mu/2)(-\mu/\eta) = \chi \Delta N_{max}/2 \tag{10}$$

Hence

$$\Delta N_{max} = 2\omega/\chi = 2\omega X \tag{11}$$

Table 6
The calculated some absorption wavelengths (λ) from 20 state, oscillator strengths (f), and frontier orbital energies of compounds **HL** and **1** by TD-DFT method in water madia (HOMO: H ve LUMO: L).

TD-DFT	Wavelengths (nm) (% Distributions)	f	MO→MO
6-311G(d, p) Water for HL	289(91%)	0.662	H→L
	217(64%)	0.094	H-1→L+2
	198(68%)	0.143	H→L+4
6-311G(d, p) Water for 1	618(76%)	0.064	H→L+3
	440(94%)	0.129	H→L+7
	362(81%)	0.203	H-1→L
	330(62%)	0.328	H→L+11

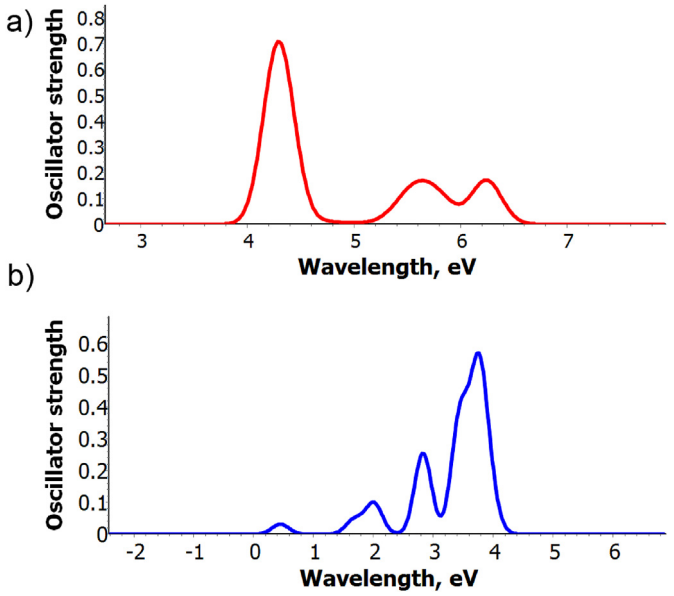

Fig. 13. The calculated UV–vis spectra by using TD-DFT/B3LYP/6-311G(d, p) in the water media **a)** for **HL**, **b)** for **1**.

Where, $X = 1/\chi$.

If we consider the two systems A and B approaching each other, the amount of charge transfer between them can be written in terms of electrophilicity, that is, electrophilicity-based charge transfer (ECT) can be written as

$$ECT = (\Delta N_{\max})_A - (\Delta N_{\max})_B = 2[\omega_A X_A - \omega_B X_B] \quad (12)$$

If ECT < 0, charge flows from A to B (A acts as an electron donor) and if ECT > 0, charge flows from B to A (A acts as an electron acceptor). It is tacitly assumed that the electrophilicity effect dominates the electronegativity effect.

The amount of charge transfer between the compounds and DNA bases (molecule: A) is calculated based on ΔN and ECT methods to know about the possible interaction of the compounds with the bases (Table 7). The values of both ΔN and ECT in Table 7 indicate that the compounds **HL** and **1** (molecule: B) act as an electron acceptor. In a reaction between two molecules, species can act as a nucleophile (electron donor), which has a lower value of the electrophilicity index. While the lowest ECT values are found in the interaction between the **HL** and **1** with the thymine base and the adenine base the largest ECT values are found in the interaction between the molecules with the guanine base. When the interactions between DNA bases and molecular structures are examined, we can say that there is a charge transfer from DNA bases to molecular structures.

4. Conclusion

In this work, a new 2-acetylpyridine derivative hydrazone ligand **HL** and its Zn(II) complex **1** have been synthesized and fully characterized using various spectroscopic methods including single crystal X-ray diffraction. Molecular structures of ligand and its zinc metal complex were investigated by DFT, one of the computational chemistry methods. X-ray diffraction analysis results show that **HL** and **1** crystallize in monoclinic and orthorhombic, respectively. The **HL** ligand behaves as mononegative tridentate with NNO donor sequence in enol form towards the metal ions. We can also say this result by looking at the change in C–N and C–O bond distances. Antibacterial activity of the compounds was assessed against Gram-positive, Gram-negative and yeast. MIC values show that the

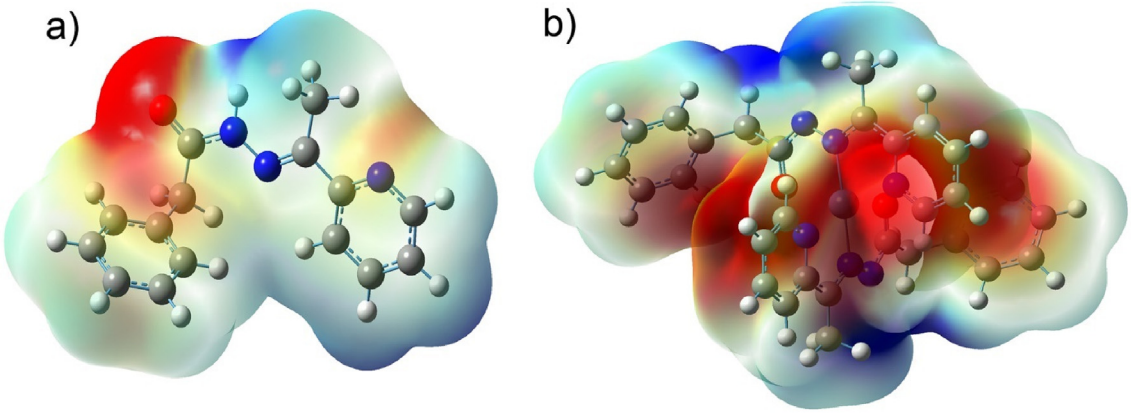

Fig. 14. MEP surface of **a) HL** and **b) 1**.

Table 7
χ, μ, η, S, ω, ΔN and ECT parameters (B: Molecule, A: DNA bases) obtained by using DFT/B3LYP/6-311G(d, p) in water media of **HL** and **1**.

	Adenine	Guanine	Cytosine	Thymine	HL	1
E_{HOMO} (eV)	−6.2393	−5.8725	−6.5515	−6.8192	−6.4587	−2.9331
E_{LUMO} (eV)	−0.8090	−0.4204	−0.9978	−1.1325	−1.8226	−2.2730
$\Delta E = E_{HOMO}$-E_{LUMO} (eV)	−5.4303	−5.4521	−5.5537	−5.6867	−4.6361	−0.6601
Total Energy (a.u.)	−467.45	−542.72	−395.06	−453.59	−820.32	−3419.98
IP (eV)	6.2393	5.8725	6.5515	6.8192	6.4587	2.9331
EA (eV)	0.8090	0.4204	0.9978	1.1325	1.8226	2.2730
μ (eV)	−3.5241	−3.1464	−3.7746	−3.9758	−4.1406	−2.6030
χ (eV)	3.5241	3.1464	3.7746	3.9758	4.1406	2.6030
η (eV)	2.7151	2.7260	2.7768	2.8433	2.3180	0.3300
S (eV^{-1})	0.1842	0.1834	0.1801	0.1758	0.2157	1.5149
ω (eV)	2.4665	1.8156	2.5660	2.7789	3.6981	10.2645
ΔN	−0.0612	−0.0985	−0.0359	−0.0160	**HL**	
ECT	−0.3864	−0.6322	−0.2133	−0.1942	**HL**	
ΔN	0.1512	0.0841	0.1885	0.2163	**1**	
ECT	−6.4868	−6.7326	−6.5288	−6.4888	**1**	

ligand was found to have more effect on *Escherichia coli*, *Bacillus cereus* and *Candida albicans* than other microorganisms. However, the complex [ZnL_2] has been found to have more effect than ligand in all microorganisms. While ligand has no significant effect on *Pseudomonas aeruginosa,* and *Salmonella typhimurium*, the complex has quite significant effects. It is thought that the synthesized new complex acts on microorganisms by disrupting the cell wall structure. In DNA cleavage study **HL** and **1** didn't show any nuclease activity in the 50 mM Tris-HCl buffer (pH: 7.2) environment. In the presence of 30 mM, H_2O_2 environment ligand didn't show any nuclease activity. But Zn complex **1** masked the hydrolytic activity of hydrogen peroxide. Because the percentage of linear form decreased and the percentage of nicked circular DNA increased. This situation explains the scavenger activity of **1** against peroxide radicals. The order of free radical scavenging activity for ligand, complex and standard increases in the order: BHA >HL > 1 >. Molecular structures have been optimized in GS gas, methanol and water environments with DFT/B3LYP/6-311G(d, p), and the optimized structures **HL** and **1** have been found to be more compatible with experimental bond parameters in the methanol media and the water media, respectively. Energy calculation results of molecular structures in different solvent environments show that the molecular structures are more stable in a more polar solvent environment. We can say that the greatest contribution of molecular structures to molecular orbital energy levels comes from pyridine and hydrazone groups. The MEP surface shows that the oxygen and the pyridine nitrogen atoms in the molecular structures exhibit the nucleophilic behavior, and the hydrazone and the methyl hydrogen atoms exhibit the electrophilic behavior. When the interaction between the molecular structures and DNA bases such as adenine, guanine, cytosine, and thymine are investigated, the obtained ECT parameters show that **HL** and **1** structures interact with the most guanine base, and charge transfer is from DNA bases to the molecular structures.

Declaration of competing interest

The authors declare that they have no known competing financial interests or personal relationships that could have appeared to influence the work reported in this paper.

CRediT authorship contribution statement

Murat Çınarlı: Conceptualization, Methodology, Resources, Investigation, Writing - review & editing. **Çiğdem Yüksektepe Ataol:** Methodology, Software, Formal analysis, Investigation, Writing - original draft, Writing - review & editing. **Esra Çınarlı:** Conceptualization, Methodology, Resources, Investigation, Writing - review & editing. **Önder İdil:** Resources, Investigation.

Appendix A. Supplementary data

Supplementary data to this article can be found online at https://doi.org/10.1016/j.molstruc.2020.128152.

References

[1] C. Sousa, C. Freire, B. de Castro, Molecules 8 (12) (2003) 894.
[2] P.V. Chalapathi, B. Prathima, Y. Subba Rao, K. Janardhan Reddy, G.N. Ramesh, D.V. Ramana Reddyand, A. Varadareddy, Res. J. Chem. Envir. 15 (2) (2011) 579.
[3] C.Z. Cheng, L. Wang, J. Liu, J. Mol. Struct. 1018 (2012) 78.
[4] L. Wang, D. Guo, Y. Wang, C. Zheng, RSC Adv. 4 (102) (2014) 58895.
[5] M. Shakir, A. Abbasi, J. Chem. Pharmaceut. Res. 7 (5) (2015) 375.
[6] Y. Zhang, L. Zhang, L. Liu, J. Guo, D. Wu, G. Xu, X. Wang, D. Jia, Inorg. Chim. Acta. 363 (2) (2010) 289.
[7] P.G. Avaji, C.H. Kumar, S.A. Patil, K.N. Shivananda, C. Nagaraju, Eur. J. Med. Chem. 44 (9) (2009) 3552.
[8] U.O. Ozmen, G. Olgun, Spectrochim. Acta, Part A 70 (3) (2008) 641.
[9] D.R. Richardson, P.V. Bernhardt, J. Biol. Inorg. Chem. 4 (3) (1999) 266.
[10] I.G. Ribeiro, K.C.M. Silva, S.C. Parrini, A.L. Ana Miranda, C.A.M. Fraga, E.J. Barreiro, Eur. J. Med. Chem. 33 (3) (1998) 225.
[11] Ş.G. Küçükgüzel, S. Rollas, I. Küçükgüzel, M. Kiraz, Eur. J. Med. Chem. 34 (12) (1999) 1093.
[12] Ş.G. Küçükgüzel, E.E. Oruç, S. Rollas, F. Şahin, A. Özbek, Eur. J. Med. Chem. 37 (3) (2002) 197.
[13] L.M. Lima, F.S. Frattani, J.L. Santos, H.J. Castro, C.A.M. Raga, R.B. Zingali, E.J. Barreiroa, Eur. J. Med. Chem. 43 (2) (2008) 348.
[14] I.M. El-Deen, A.F. Shoair, M.A. El-Bindary, J. Mol. Struct. 1180 (2019) 420.
[15] H.A. Sahyon, A.A. El-Bindary, A.F. Shoair, A.A. Abdellatif, J. Mol. Liq. 255 (2018) 122.
[16] A.F. Shoair, A.A. El-Bindary, N.A. El-Ghamaz, G.N. Rezk, J. Mol. Liq. 269 (2018) 619.
[17] W. Cao, Y. Liu, T. Zhang, J. Jia, Polyhedron 147 (2018) 62.
[18] A.Z. El-Sonbati, M.A. Diab, ShM. Morgan, M.I. Abou-Dobara, A.A. El-Ghettany, J. Mol. Struct. 1200 (2020) 127065.
[19] M.I. Abou-Dobara, N.F. Omar, M.A. Diab, A.Z. El-Sonbati, ShM. Morgan, M.A. El-Mogazy, Mater. Sci. Eng. C 103 (2019) 109727.
[20] A.Z. El-Sonbati, M.A. Diab, A.M. Eldesoky, ShM. Morgan, O.L. Salem, Appl. Organomet. Chem. 33 (2019) e4839.
[21] M.A. Diab, A.Z. El-Sonbati, ShM. Morgan, M.A. El-Mogazy, Appl. Organomet. Chem. 32 (2018) e4378.
[22] A.Z. El-Sonbati, M.A. Diab, ShM. Morgan, A.M. Eldesoky, M.Z. Balboula, Appl. Organomet. Chem. 32 (2018), e4207.
[23] ShM. Morgan, M.A. Diab, A.Z. El-Sonbati, Appl. Organomet. Chem. 32 (2018), e4305.
[24] ShM. Morgan, A.Z. El-Sonbati, H.R. Eissa, J. Mol. Liq. 240 (2017) 752.
[25] A.Z. El-Sonbati, M.A. Diab, ShM. Morgan, J. Mol. Liq. 225 (2017) 195.
[26] A.Z. El-Sonbati, M.A. Diab, ShM. Morgan, H.A. Seyam, J. Mol. Struct. 1154 (2018) 354.
[27] ShM. Morgan, M.A. Diab, A.Z. El-Sonbati, Appl. Organomet. Chem. 32 (2018), e4281.
[28] M.I. Abou-Dobara, A.Z. El-Sonbati, ShM. Morgan, World J. Microbiol. Biotechnol. 29 (2013) 119.
[29] M.A. Diab, Gehad G. Mohamed, W.H. Mahmoud, A.Z. El-Sonbati, ShM. Morgan, S.Y. Abbas, Appl. Organomet. Chem. 33 (2019) e4945.

[30] A.Z. El-Sonbati, W.H. Mahmoud, G.G. Mohamed, M.A. Diab, ShM. Morgan, S.Y. Abbas, Appl. Organomet. Chem. 33 (2019) e5048.
[31] ShM. Morgan, M.A. Diab, A.Z. El-Sonbati, Appl. Organomet. Chem. 32 (2018), e4504.
[32] H.M. Refaat, H.A. El-Badway, ShM. Morgan, J. Mol. Liq. 220 (2016) 802.
[33] G.G. Mohamed, A.A. El-Sherif, M.A. Saad, S.E.A. El-Sawy, ShM. Morgan, J. Mol. Liq. 223 (2016) 1311.
[34] C. Yao Lin, L.C. Chuang, G.H. Lee, S.M. Peng, J. Org. Chem. 690 (1) (2005) 244.
[35] X.S. Tai, H. Wang, X. Sun, M. Tan, Spectrosc. Lett. 38 (4–5) (2005) 497.
[36] U. Abram, C.C. Gatto, E. Bonfada, E.S. Lang, Inorg. Chem. Commun. 5 (7) (2002) 461.
[37] M. Fondo, A. Sousa, M.R. Bermejo, A.G. Deibe, A.S. Pedrares, O.L. Hoyos, M. Helliwell, Eur. J. Inorg. Chem. 3 (2002) 703.
[38] A.D. Becke, J. Chem. Phys. 98 (1993) 5648.
[39] C. Lee, W. Yang, R.G. Parr, Phys. Rev. B37 (1988) 785.
[40] M.J. Frisch, G.W. Trucks, H.B. Schlegel, G.E. Scuseria, M.A. Robb, J.R. Cheeseman, G. Scalmani, V. Barone, B. Mennucci, G.A. Petersson, H. Nakatsuji, M. Caricato, X. Li, H.P. Hratchian, A.F. Izmaylov, J. Bloino, G. Zheng, J.L. Sonnenberg, M. Hada, M. Ehara, K. Toyota, R. Fukuda, J. Hasegawa, M. Ishida, T. Nakajima, Y. Honda, O. Kitao, H. Nakai, T. Vreven, J.A. Montgomery Jr., J.E. Peralta, F. Ogliaro, M. Bearpark, J.J. Heyd, E. Brothers, K.N. Kudin, V.N. Staroverov, R. Kobayashi, J. Normand, K. Raghavachari, A. Rendell, J.C. Burant, S.S. Iyengar, J. Tomasi, M. Cossi, N. Rega, J.M. Millam, M. Klene, J.E. Knox, J.B. Cross, V. Bakken, C. Adamo, J. Jaramillo, R. Gomperts, R.E. Stratmann, O. Yazyev, A.J. Austin, R. Cammi, C. Pomelli, J.W. Ochterski, R.L. Martin, K. Morokuma, V.G. Zakrzewski, G.A. Voth, P. Salvador, J.J. Dannenberg, S. Dapprich, A.D. Daniels, €O. Farkas, J.B. Foresman, J.V. Ortiz, J. Cioslowski, D.J. Fox, Gaussian 09, Gaussian, Inc., Wallingford (CT, USA), 2009.
[41] G.M. Sheldrick, Acta Crystallogr. A**71** (2015) 3.
[42] L.J. Farrugia, J. Appl. Crystallogr. 45 (2012) 849.
[43] G.M. Sheldrick, Acta Crystallogr. C**71** (2015) 3.
[44] A. Shahzad, Z. Gul, E. Khan, M.N. Umar, M.R. Shah, A. Noor, S.W. Khan, Quím. Nova 48 (8) (2017) 902.
[45] X.-Y. Zhang, X.-L. Hanband, Z.-B. Qianc, Acta Crystallogr. E68 (2012) o3203.
[46] M. Çınarlı, E. Çınarlı, Ç. Yüksektepe Ataol, Ö. İdil, E. Kariptaş, J. Mol. Struct. 1196 (2019) 760.
[47] M. Çınarlı, Ç. Yüksektepe Ataol, H. Batı, F. Güntepe, H. Öğütçü, O. Büyükgüngör, Inorg. Chim. Acta. 484 (2019) 87.
[48] Ş. Karadeniz, Ç. Yüksektepe Ataol, T. Özen, R. Demir, H. Öğütçü, H. Batı, J. Mol. Struct. 1175 (2019) 39.
[49] A. Zülfikaroglu, Ç. Yüksektepe Ataol, E. Çelikoglu, U. Çelikoglu, O. İdil, J. Mol. Struct. 1199 (2020) 127012.
[50] S. Demir, M. Dinçer, A. Çukurovali, I. Yılmaz, Crystallogr. Rep. 62 (6) (2017) 868.
[51] S.D. Kanmazalp, M. Macit, N. Dege, J. Mol. Struct. 1179 (2019) 181.
[52] A. Zülfikaroglu, H. Batı, N. Dege, J. Mol. Struct. 1162 (2018) 125.
[53] A. Zülfikaroglu, J. Mol. Struct. 1209 (2020) 127950.
[54] Ş. Karadeniz, Ç. Yüksektepe Ataol, O. Şahin, Ö. İdil, H. Batı, J. Mol. Struct. 1161 (2018) 477.
[55] D.B. Wang, B.H. Chen, Y.X. Ma, Synt. Reac. Inorg. Metal-Org. Chem. 27 (4) (1997) 479.
[56] A. Ray, S. Banerjee, S. Sen, R.J. Butcher, G.M. Rosair, M.T. Garland, S. Mitra, Struct. Chem. 19 (2) (2008) 209.
[57] Z.-Q. Liu, Y.M. Ng, P.J. Tiong, R.A.A. Talip, N. Jasin, V.Y.M. Jong, M.G. Tay, Int. J. Inorg. Chem. 2017 (2017) 7520640.
[58] G. Borkow, J. Gabbay, Curr. Med. Chem. 12 (18) (2005) 2163.
[59] T.N. Phan, T. Buckner, J. Sheng, J.D. Baldeck, R.E. Marquis, Oral Microbiol. Immunol. 19 (1) (2004) 31.
[60] A.A. El-Sherif, T.M.A. Eldebss, Spectrochim. Acta, Part A 79 (5) (2011) 1803.
[61] Z. Demircioglu, G. Kastaş, Ç. Albayrak Kaştaş, R. Frank, J. Mol. Struct. 1191 (2019) 129.
[62] R.G. Pearson, Chemical Hardnesss Applications from Molecules to Solids, VCH-Wiley, Weinheim, Germany, 1997.
[63] R.G. Parr, W. Yang, Density Functional Theory of Atoms and Molecules, Oxford University Press, Oxford, U.K, 1989.
[64] R.P. Iczkowski, J.L. Margrave, J. A. Chem. Soc. 83 (1961) 3547.
[65] R.G. Parr, R.G. Pearson, J. A. Chem. Soc. 105 (1983) 7512.